Steady decline in mean annual air temperatures in the first 30 ka after the Cretaceous-Paleogene boundary

Lauren K. O'Connor[1]*^, Emily Dearing Crampton-Flood[1]^, Rhodri M. Jerrett[1], Gregory D. Price[2], B. David A. Naafs[3], Richard D. Pancost[3], Paul McCormack[2], Aris Lempotesis-Davies[1], Bart E. van Dongen[1], and Sabine K. Lengger[2,4]

[1]Department of Earth and Environmental Sciences, University of Manchester, Oxford Road, Manchester, M13 9PL, UK

[2]School of Geography, Earth and Environmental Sciences, Plymouth University, Drake Circus, Plymouth, PL4 8AA, UK

[3]School of Chemistry, School of Earth Sciences, Cabot Institute for the Environment, University of Bristol, BS8 1TS Bristol, UK

[4]Sensor Systems Division, Silicon Austria Labs, Villach 9524, Austria

^Joint first-authorship

Correspondence to: lauren.oconnor@manchester.ac.uk

This paper is a non-peer reviewed preprint submitted to EarthArXiv and has been submitted to *Geology* for peer review.

Steady decline in mean annual air temperatures in the first 30 ka after the Cretaceous-Paleogene boundary

Lauren K. O'Connor[1]*^, Emily Dearing Crampton-Flood[1]^, Rhodri M. Jerrett[1], Gregory D. Price[2], B. David A. Naafs[3], Richard D. Pancost[3], Paul McCormack[2], Aris Lempotesis-Davies[1], Bart E. van Dongen[1], and Sabine K. Lengger[2,4]

[1]Department of Earth and Environmental Sciences, University of Manchester, Oxford Road, Manchester, M13 9PL, UK

[2]School of Geography, Earth and Environmental Sciences, Plymouth University, Drake Circus, Plymouth, PL4 8AA, UK

[3]School of Chemistry, School of Earth Sciences, Cabot Institute for the Environment, University of Bristol, BS8 1TS Bristol, UK

[4]Sensor Systems Division, Silicon Austria Labs, Villach 9524, Austria

^Joint first-authorship

Correspondence to: lauren.oconnor@manchester.ac.uk

ABSTRACT

The Cretaceous-Paleogene (K-Pg) boundary marks one of the five major mass extinctions of the Phanerozoic. How the climate system responded to a bolide impact and extensive volcanism at this time over different timescales is highly debated. Here we use the distribution of branched tetraether lipids (brGDGT) from fossil peats at two sites in Saskatchewan, Canada (paleolatitude ~55°N), to generate a high-resolution (millennial) record of mean annual air temperature (MAAT) spanning the last ~4 ka of the Cretaceous and first ~30 ka of the Paleogene. Our study shows that MAATs ranged from 16–29°C, with the highest value in the first millennia of the Paleogene/ The earliest Paleogene averaged ~25°C—maintaining or enhancing warmth from the latest Cretaceous—

followed by a general cooling to ~20°C over the following ~30 ka. No abrupt post-boundary cooling (e.g., an "impact winter") or abrupt warming are evident in our data, implying that if such phenomena occurred, their duration was relatively short-lived (i.e., sub-millennial). Further, no long-term impact- or volcanism-driven warming is evident. The range of temperature change observed is considerably greater than that derived from marine proxy records over the same time interval. Our findings therefore more properly place bounds on the magnitude and duration of temperature change on land during this critical interval—the main setting for the demise of non-avian dinosaurs and the rise of mammals.

INTRODUCTION

The Cretaceous-Paleogene (K-Pg) boundary marks one of the five major mass extinctions of the Phanerozoic. Climate change triggered by a bolide impact on the Yucatán Peninsula and Deccan Trap volcanism is implicated in the mass extinction, but how different parts of the climate system responded to these triggers and at what timescales remains highly debated (e.g., Schoene et al. 2019; Sprain et al. 2019; Hull et al. 2020). Both the impact and volcanism have spurred numerous models of their effect on climate, but tests of these hypotheses are hampered, in part, by a lack of sufficiently resolved temperature constraints close to the boundary itself, especially from the terrestrial realm.

Bolide impact models suggest an intense heat pulse in the first minutes to hours after impact caused by the return flux of larger ejecta and flash heating of the atmosphere (Lewis et al. 1982; Melosh et al. 1990); an "impact winter" lasting months to millennia due to atmospheric loading of dust, soot, and sulfate aerosols (Pope et al. 1994; Bardeen et al. 2017; Brugger et al. 2017); and global warming caused by CO_2 from impact-volatilized carbonates (and wildfires) beginning 10^3 years after impact (O'Keefe and Ahrens 1989). Establishing a relationship between Deccan volcanism and climate change at the K-Pg boundary is limited by difficulties in dating the lava flows (Schoene et al. 2019; Sprain et al. 2019) and constraining the amount and rate of associated CO_2 and SO_2 release (Self et al. 2006; Schmidt et al. 2016). Nevertheless, a compilation of global temperature records across the K-Pg

boundary (Hull et al. 2020) shows that: (1) an episode of warming (~2°C) between 350 and 200 ka before the K-Pg boundary was coincident with the onset of volcanism; (2) a subsequent decline in temperatures lasted until the boundary itself, likely driven by absorption of CO_2 into the ocean following the cessation of outgassing; and (3) the first 1 Ma of the Paleocene was characterized by warming of ~1°C. Discrete reconstructions of temperature change at the K-Pg boundary at higher temporal resolution are confined to shallow-marine records (e.g., Vellekoop et al. 2014). High-resolution air temperature data are required to develop a holistic understanding of the global response to events at the K-Pg boundary, and to contextualize climate change on land.

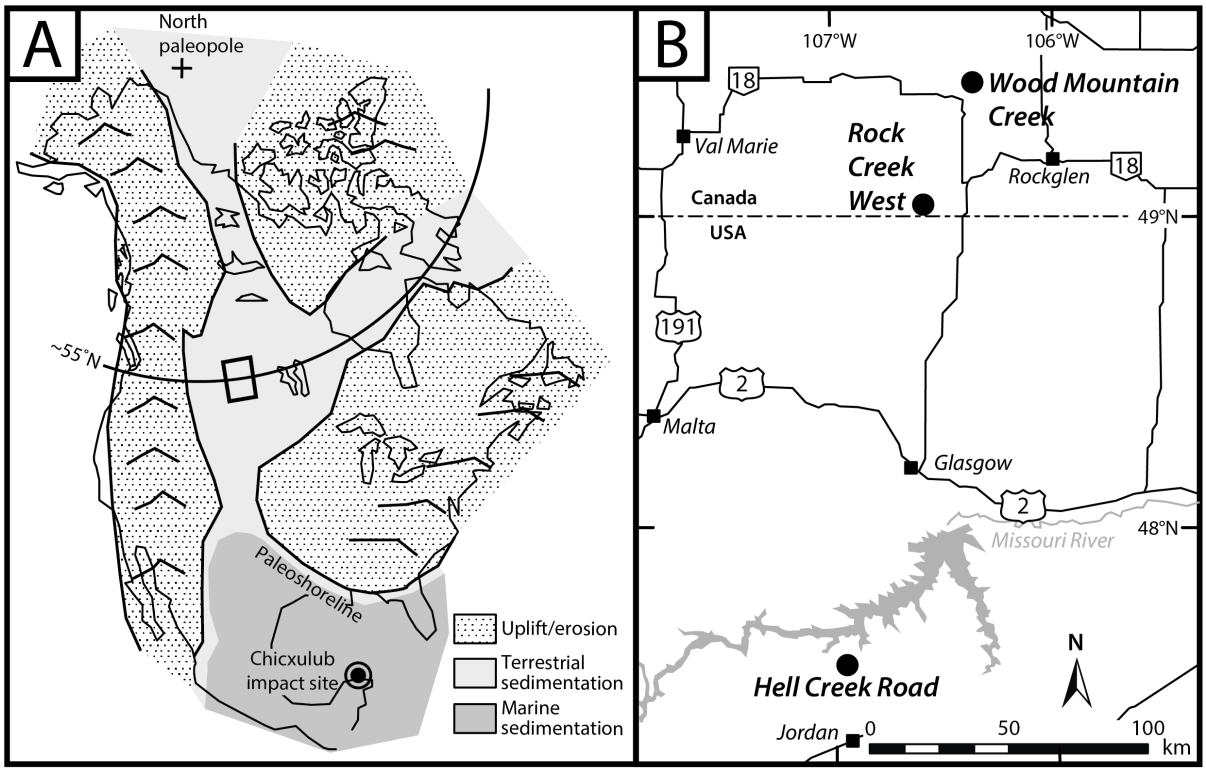

Figure 1. *[A] Cretaceous-Paleogene paleogeography of North America (based on Smith et al. 1981 and van Hinsbergen et al. 2015) and study area in [B] outlined by black box. [B] Inset of study area with modern geography showing the locations of sites named in this study. We use samples from Wood Mountain Creek and Rock Creek West.*

In this study, we apply a lipid biomarker paleotemperature proxy (MBT'_{5Me}; Weijers et al. 2007; De Jonge 2014; Naafs et al. 2017) to fossil peats (coals) to reconstruct mean annual air temperatures (MAAT) at a millennial resolution across the K-Pg boundary. The coals are from two sites located 45 km apart—Wood Mountain Creek and Rock Creek West (Saskatchewan, Canada)—which lay at a paleolatitude of 54–56°N at the time of deposition (van Hinsbergen et al. 2015; Fig. 1). Both coals contain the distinctive Ir-enriched claystone, palynological extinction, and fern-spore spike that globally mark the boundary (Sweet and Braman 1992). The Ir-anomaly claystone and $\delta^{13}C_{org}$ stratigraphies of the coals are used to correlate the two sites and produce a composite MAAT record. These data allow the testing, for the first time, of hypothesized terrestrial climate change at the K-Pg boundary at the timescales of 10^3 to 10^4 years.

APPROACH AND METHODS

The MBT'_{5Me} proxy is based on branched glycerol dialkyl glycerol tetraethers (brGDGTs), which are membrane lipids produced by bacteria (Chen et al. 2022; Halamka et al. 2022). The degree of methylation of these branched tetraethers (MBT) is dependent on the temperature at which the molecule was metabolized (Weijers et al. 2007; De Jonge et al 2014; Chen et al. 2022), allowing for their use as a MAAT proxy, applied as far back as the Paleogene (Naafs et al. 2018).

Coals from Wood Mountain Creek (49°25’20”N 106°19’50”W) and Rock Creek West (49°02’20”N 106°34’00”W) were sampled contiguously, and freeze-dried and powdered for geochemical analysis (Supplementary Material). Samples were solvent extracted, and the total lipid extracts (Wood Mountain Creek) or polar fractions (Rock Creek West) were dissolved in hexane:isopropanol (99:1, v/v) and filtered (0.45 µm PTFE) prior to analysis by high performance liquid chromatography-atmospheric pressure chemical ionization-mass spectrometry (HPLC/APCI-MS) on a ThermoFisher Scientific Accela Quantum Access triple quadrupole (Wood Mountain Creek, University of Bristol) and a TSQ Quantum Access Orbitrap HPLC-MS (Rock Creek West, University of Plymouth; Vickers et al. 2020). The apolar fractions were then analyzed using an Agilent 5975C gas

chromatograph with an Agilent 5975C MSD mass spectrometer. Bulk organic $\delta^{13}C$ analyses were conducted at Plymouth University using an Isoprime mass spectrometer connected to an Isoprime Microcube elemental analyzer.

TEMPERATURE DATA, CORRELATION, AND AGE MODEL

The brGDGT distributions from both sites show similar MBT'_{5me} values, which translate to MAATs (Naafs et al. 2017) ranging from 16.7–27.9 ±4.7°C at Rock Creek West and 14.4–29.1 ±4.7°C at Wood Mountain Creek (Fig. S2). The similarity in the two records, in both absolute values and trends, provides confidence in the fidelity of the individual records. $\delta^{13}C$ values at both sites are similar (-25.5 to -21.1‰ at Rock Creek West and -27.2 to -21.9‰ at Wood Mountain Creek), and show recognizable excursions with similar shapes and magnitudes that allow for reliable correlation between the sites (Fig. 2). The Ir-enriched claystone is used as the primary datum for correlation between the two sites. The inflexion points on the $\delta^{13}C$ curves are used as secondary, independent, tie points to produce the composite temperature record (Fig. 3).

Notwithstanding likely differences in rates of peat accumulation and/or compaction between the two sites, it is possible to place bounds on the duration of time represented by the composite record. Absolute age determinations of two tuffs by Renne et al. (2013) at a contemporaneous coal-bearing K-Pg site (Hell Creek Marina Road, Montana), located 170 km SSW of Rock Creek West (Fig. 1), yield for 1 m of coal a most likely duration of ~40 ka (with a maximum duration of up to 175 ka, and an unlikely minimum duration that equates to instantaneous deposition (Supplementary Material). However, modelling of the timing of impact debris fall-out (Goderis et al. 2021), and estimates of the duration of time represented by the fern-spore spike (Clyde et al. 2016) contained within the Ir-enriched impact claystone (Sweet and Braman 1992), imply that the first MAAT datapoint above it must represent at least ~1 ka after bolide impact at the K-Pg boundary (Fig. 3). We use the value for the most likely duration (1 m of coal = 40 ka) to estimate time at our two sites, but continue to acknowledge the uncertainty outlined above (Fig. 3).

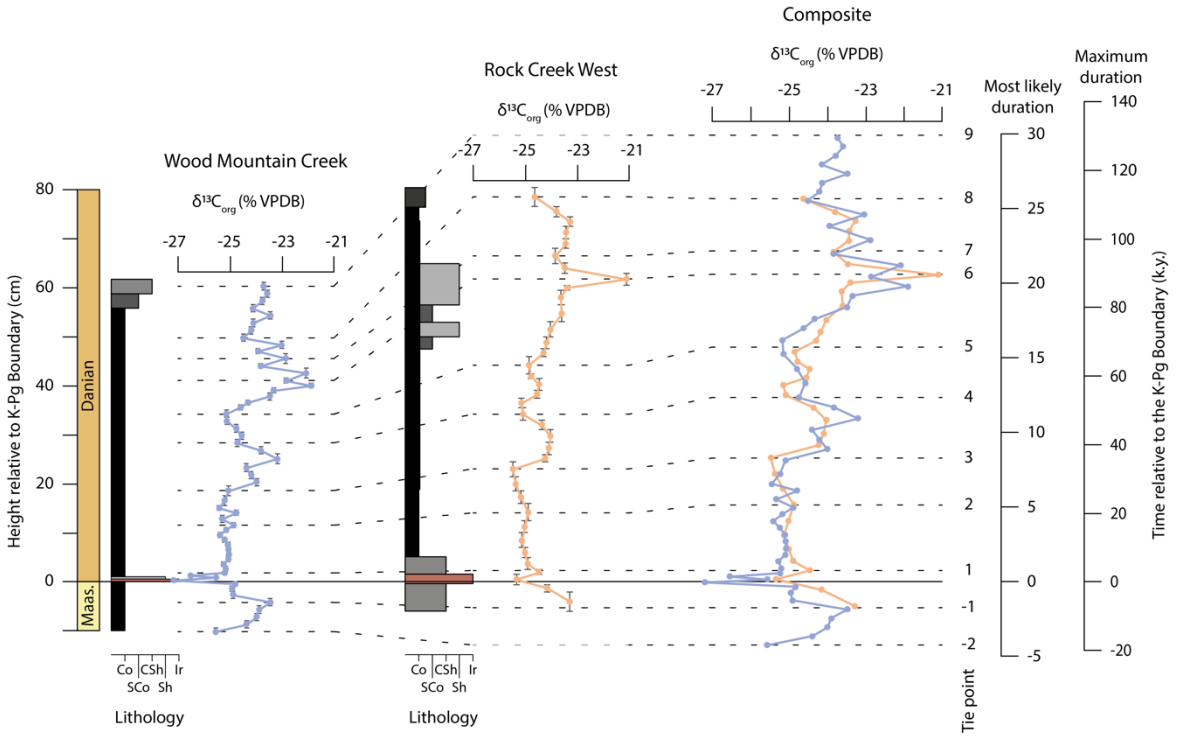

Figure 2. *$\delta^{13}C_{org}$ records from Wood Mountain Creek (blue) and Rock Creek West (orange), Saskatchewan, plotted against height above the K-Pg boundary. Vertical error bars show the stratigraphic range of each sample. Dashed lines show chemostratigraphic ($\delta^{13}C$) correlation tiepoints numbered 1–9 (Supplementary Table S3). Solid line shows the Ir-claystone K-Pg datum. The composite record is plotted against time, with the most likely (40 ka/m of coal) and maximum (175 ka/m of coal) durations shown. On the lithology log, Co = coal, ShC = shaley coal, CSh = coaly shale, Sh = shale, and Ir = iridium-enriched claystone.*

Given the difficulty in constraining age in such a high-resolution section, and the large paleotemperature calibration error, we treat detail in our MAAT record cautiously: we focus on the most pronounced trends and have binned the data into 10-ka intervals. Our composite record (Fig. 3) shows general warmth in the latest Cretaceous, albeit with scatter (avg. = 24.5°C ±2.7, n = 7), which increased to the highest MAATs (avg. = 25.2°C ±2.0, n = 21) in the first 10 ka after the K-Pg boundary ($p = 0.13$). The subsequent 10 ka interval experienced a general decline in temperatures (avg. = 22.8°C

±1.8, n = 22, p = 0.00), followed by a continued decline to 20.4°C (±2.7, n = 19, p = 0.00) over the remaining 10 ka of our record.

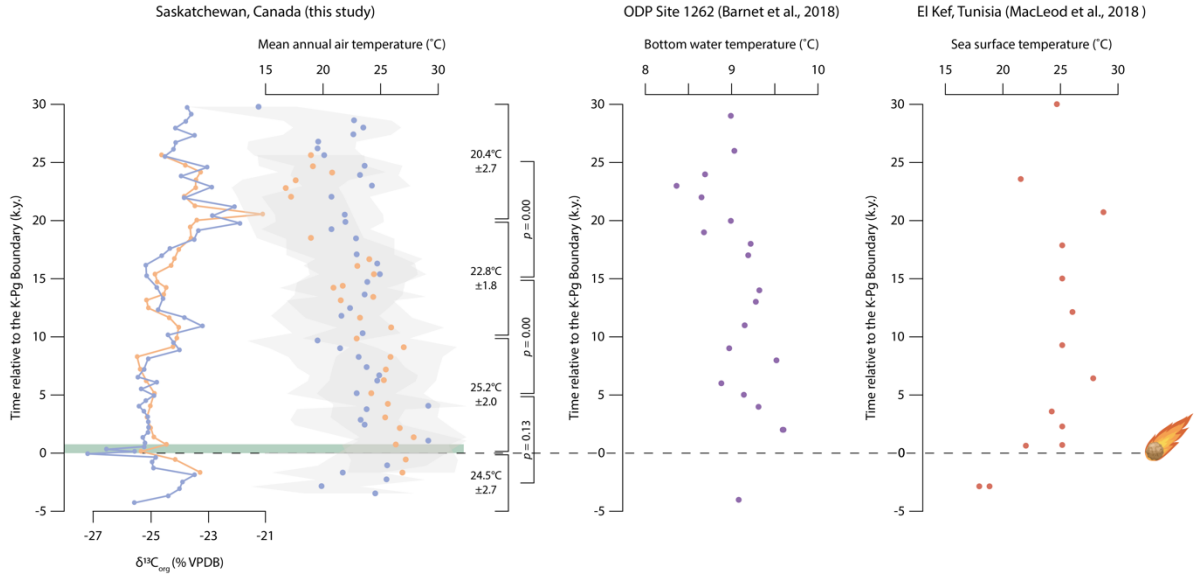

Figure 3. *Composite $\delta^{13}C_{org}$ and mean annual air temperature (MAAT) records from Wood Mountain Creek (blue) and Rock Creek West (orange) plotted against time relative to the K-Pg boundary (using the most likely duration), compared with the $\delta^{18}O$ temperature data of Barnet et al. (2017) and MacLeod et al. (2018) over the same time interval. The dashed line represents the K-Pg boundary. Average MAATs ± standard deviations for each temporal bin are shown to the right with P values of t tests comparing means (Table S5). The green bar represents at least ~1 ka after bolide impact at the K-Pg boundary during which we lack data.*

DISCUSSION

The absolute MAATs (17–29°C) and binned averages (20–25°C) are more than 10°C higher than modern MAATs at the equivalent latitude in the western interior of North America. However, these data agree with general circulation models (e.g., Sellwood and Valdes 2006; Tabor et al. 2016) and other terrestrial proxy data (Zhang et al. 2019) that indicate temperatures of 20°C in the Arctic to

30°C at the southern margin of the North American western interior across the K-Pg boundary. These new data support the hypothesis of a reduced latitudinal temperature gradients at this time.

Several other observations stand out from the Saskatchewan record. Firstly, neither abrupt warming nor cooling are observed immediately post-impact. Latest Cretaceous warmth was weakly enhanced by 0.7°C between the last ~4 ka of the Cretaceous and first ~10 ka of the Paleogene (Fig. 3). Climate models suggest that the impact winter lasted only years to decades (Pope et al. 1994; Tabor et al. 2016; Bardeen et al. 2017), which is below the resolution of our record. Our data therefore do not preclude a brief episode of post-impact cooling at the timescales indicated by these models. However, our data do not support the notion of abrupt, impact winter lasting more a thousand years, as interpreted from the shallow-marine record of Vellekoop et al. (2014). The cooling observed in their record occurs within the interpreted fall-out of the waning tail of a tsunami, which, irrespective of linear time-interpolation models, represents a geologically instantaneous event bed. Further, the origin of organic matter within such deposits should also be treated with caution, given the potential of such flows to entrain and transport (older) sediment from marine and terrestrial environments, potentially biasing this proxy record.

There is no evidence for abrupt global warming sustained over 10^4–10^5 years as suggested by some models (O'Keefe and Ahrens 1989), and purportedly supported by marine (MacLeod et al. 2018; Taylor et al. 2018) and terrestrial (Lyson et al. 2019) proxy data. Although the highest individual MAAT datapoints of our record occur in within the first 10 ka of the Paleogene, our data suggest this interval was preceded by general warming in the last 5 ka of the Cretaceous (Fig. 3). This trend is also evident in the relatively high-resolution benthic $\delta^{18}O$ record of Barnet et al. (2017). The “abrupt” 3–5°C of warming observed in other records (MacLeod et al. 2018; Lyson et al. 2019) may be an artifact of low-resolution spot-sampling, as in even the highest-resolution records (Barnet et al. 2017; MacLeod et al. 2018) there is a gap of no less than ~3 ka between the last Cretaceous datapoint and the K-Pg boundary itself (Fig. 3). The data from these studies are consistent with our results, insofar as there is a temperature increase across the K-Pg boundary, but we posit that these values represent the

culmination of a longer-term warming trend—pre-dating the bolide impact—and cannot be considered “abrupt”. Although bolide impact is inextricably linked to the mass extinction, its effect on terrestrial temperatures appears to have been modest at most: either weakly enhancing an already existing latest Cretaceous warmth or failing to interrupt the pre-existing trend of latest Cretaceous warming, or the post-boundary temperature trends (or their geographical expression) are more complex than previously thought.

Early Paleogene warmth cannot be said to be “sustained” at the timescales implied by models of global warming caused by impact-volatilization (O’Keefe and Ahrens, 1989) in our data. Irrespective of the most likely (30 ka) or longest possible (130 ka) duration for our earliest Paleogene record, we document a gradual decline in MAAT in the tens of thousands of years that follow the K-Pg boundary (Fig. 3). The marine $\delta^{18}O$ records of Barnet et al. (2019) from the South Atlantic documents 1–2°C of cooling over ~30 ka. Another, from the Tethyan K-Pg type section at El Kef, Tunisia (MacLeod et al. 2018) shows sustained warmth for ~100 ka followed by up to 5°C of cooling over ~100 ka. The timescales of cooling in these studies are within the error margin of this study and one-another. Similarly, from the terrestrial realm, lower-resolution paleobotanical studies from the western interior of North America that indicate lower temperatures relative to the latest Cretaceous mean within the first ~100 kyr of the Paleogene (Lyson et al. 2019 and references therein). Overall, data converge on the notion of temperature maxima immediately following the K-Pg boundary, followed by several tens of thousands of years, at least, of cooling in the earliest Paleogene.

Finally, relative to comparable marine records, the magnitude (up to 5°C in the binned data) of MAAT change in our data is greater than that of Barnet et al. (2017), but similar to that of MacLeod et al. (2018). Owing to the different thermal masses of land and ocean, differences in the magnitude and duration of temperature change in response to external drivers might be expected (Sutton et al. 2007). Understanding and quantifying these differences is limited by the error margins of age models and temporal resolution of existing data. As such, the generation of directly comparable, time-

calibrated marine and terrestrial archives is critical to a holistic understanding of the evolution of the ocean-atmosphere system across the K-Pg boundary.

CONCLUSION

We observe similar absolute values and trends of terrestrial temperature change across the K-Pg boundary at two closely spaced fossil peats that were located at ~55°N in what is now southern Saskatchewan. This similarity has permitted the generation of a millennial-scale, composite MAAT record through this critical time interval. MAATs peaked at ~25°C within the first ~10 ka of the Paleogene, which we tentatively interpret to represent the weak enhancement of warmth from the last ~4 ka of the Cretaceous. Peak warmth was followed by ~5°C cooling over the following 20 ka. We observe no "impact winter" nor a spike in temperature immediately following the boundary. If such phenomena occurred, their duration was below the resolution of our record: ~1 ka. Our data highlight the value of peat as a sensitive, high-resolution paleotemperature archive, and place new bounds on the magnitude and rate of millennial-scale MAAT change in the terrestrial realm—the main setting for the demise of non-avian dinosaurs and the rise of mammals occurred.

ACKNOWLEDGEMENTS

The study was funded by UK Natural Environment Research Council grant NE/S002324/1 awarded to RJM. BDAN also acknowledges funding through a Royal Society Tata University Research Fellowship. Thanks to Grasslands National Park for allowing access to Rock Creek West, and Ritchie Hordenchuk for access to Wood Mountain Creek. Thanks to Steve Stockley, Abby Ragazzon-Smith, and Paul Lythgoe (University of Manchester), Marc Davies and Steve Rowland (University of Plymouth), and Ian Bull (University of Bristol) for technical assistance.

REFERENCES

Bardeen, C. G., Garcia, R. R., Toon, O. B., and Conley, A. J., 2017, On transient climate change at the Cretaceous−Paleogene boundary due to atmospheric soot injections: Proceedings of the National Academy of Sciences, v. 114, p. E7415-E7424, doi: 10.1073/pnas.1708980114.

Barnet, J. S., Littler, K., Westerhold, T., Kroon, D., Leng, M. J., Leng, M.J., Bailey, I., Röhl, U. and Zachos, J.C., 2019, A high-Fidelity benthic stable isotope record of late Cretaceous–early Eocene climate change and carbon-cycling: Paleoceanography and Paleoclimatology, v. 34, p. 672-691, doi: 10.1029/2019pa003556.

Brugger, J., Feulner, G., and Petri, S., 2017, Baby, it's cold outside: Climate model simulations of the effects of the asteroid impact at the end of the Cretaceous: Geophysical Research Letters, v. 44, p. 419-427, doi: 10.1002/2016gl072241.

Chen, Y., Zheng, F., Yang, H., Yang, W., Wu, R., Liu, X., Liang, H., Chen, H., Pei, H., Zhang, C., Pancost, R.D., Zeng, Z., 2022, The production of diverse brGDGTs by an Acidobacterium providing a physiological basis for paleoclimate proxies: Geochimica et Cosmochimica Acta, v. 337, p. 155-165, doi: 10.1016/j.gca.2022.08.033.

Clyde, W. C., Ramezani, J., Johnson, K. R., Bowring, S. A., and Jones, M. M. (2016). Direct high-precision U–Pb geochronology of the end-Cretaceous extinction and calibration of Paleocene astronomical timescales. Earth and Planetary Science Letters, v. 452, p. 272-280, doi: 10.1016/j.epsl.2016.07.041.

De Jonge, C., Hopmans, E. C., Zell, C. I., Kim, J. H., Schouten, S., and Damsté, J. S. S., 2014, Occurrence and abundance of 6-methyl branched glycerol dialkyl glycerol tetraethers in soils: Implications for palaeoclimate reconstruction: Geochimica et Cosmochimica Acta, v. 141, p. 97-112, doi: 10.1016/j.gca.2014.06.013.

Gooderis, S., et al., 2021, Globally distributed iridium layer preserved within the Chicxulub impact structure: Science Advances, v. 7, p. eabe3647, doi: 10.1126/sciadv.abe3647.

Hull, P. M., et al., 2020, On impact and volcanism across the Cretaceous-Paleogene boundary: Science, v. 367, p. 266-272, doi: 10.1126/science.aay5055.

Inglis, G. N., Farnsworth, A., Collinson, M. E., Carmichael, M. J., Naafs, B. D. A., Lunt, D. J., Valdes, P.J. and Pancost, R.D., 2019, Terrestrial environmental change across the onset of the PETM and the associated impact on biomarker proxies: A cautionary tale: Global and Planetary Change, v. 181, 102991, doi: 10.1016/j.gloplacha.2019.102991.

Lewis, J., Watkins, H., Hartman H., and Prinn, R., 1982, Chemical consequences of major impacts on Earth: Geological Society of America Special Paper 190, p. 215-221, doi: 10.1130/spe190-p215.

Lyson, T. R., et al., 2019, Exceptional continental record of biotic recovery after the Cretaceous–Paleogene mass extinction. Science, v. 366, p. 977-983, doi: 10.1126/science.aay2268.

MacLeod, K. G., Quinton, P. C., Sepúlveda, J., and Negra, M. H., 2018, Postimpact earliest Paleogene warming shown by fish debris oxygen isotopes (El Kef, Tunisia): Science, v. 360, p. 1467-1469, doi: 10.1126/science.aap8525.

Melosh, H. J., Schneider, N. M., Zahnle, K. J., and Latham, D., 1990, Ignition of global wildfires at the Cretaceous/Tertiary boundary: Nature, v. 343, p. 251-254, doi: 10.1038/343251a0.

Naafs, B.D.A., et al., 2017, Introducing global peat-specific temperature and pH calibrations based on brGDGT bacterial lipids: Geochimica et Cosmochimica Acta, v. 208, p. 285-301, doi: 10.1016/j.gca.2017.01.038.

Naafs, B. D. A., et al., 2018, High temperatures in the terrestrial mid-latitudes during the early Palaeogene: Nature Geoscience, v. 11, p. 766-771, doi: 10.1038/s41561-018-0199-0.

O'Keefe, J. D., and Ahrens, T. J., 1989, Impact production of CO2 by the Cretaceous/Tertiary extinction bolide and the resultant heating of the Earth: Nature, v. 338, p. 247-249, doi: 10.1038/338247a0.

297 Pope, K. O., Baines, K. H., Ocampo, A. C., and Ivanov, B. A., 1994, Impact winter and the
298 Cretaceous/Tertiary extinctions: Results of a Chicxulub asteroid impact model: Earth and
299 Planetary Science Letters, v. 128, p. 719-725, doi: 10.1016/0012-821X(94)90186-4.

300 Renne, P. R., Deino, A. L., Hilgen, F. J., Kuiper, K. F., Mark, D. F., Mitchell III, W. S., Morgan, L.E., Mundil,
301 R. and Smit, J., 2013, Time scales of critical events around the Cretaceous-Paleogene boundary:
302 Science, v. 339, p. 684-687, doi: 10.1126/science.1230492.

303 Schmidt, A., et al., 2016, Selective environmental stress from sulphur emitted by continental flood
304 basalt eruptions. Nature Geoscience, v. 9, p. 77-82, doi: 10.1038/ngeo2588.

305 Schoene, B., Eddy, M. P., Samperton, K. M., Keller, C. B., Keller, G., Adatte, T., and Khadri, S. F., 2019,
306 U-Pb constraints on pulsed eruption of the Deccan Traps across the end-Cretaceous mass
307 extinction: Science, v. 363, p. 862-866, doi: 10.1126/science.aau242.

308 Self, S., Widdowson, M., Thordarson, T., and Jay, A. E., 2006, Volatile fluxes during flood basalt
309 eruptions and potential effects on the global environment: A Deccan perspective: Earth and
310 Planetary Science Letters, v. 248, p. 518-532, doi: 10.1016/j.epsl.2006.05.041.

311 Sellwood, B. W., and Valdes, P. J., 2006, Mesozoic climates: General circulation models and the rock
312 record: Sedimentary Geology, v. 190, p. 269-287, doi: 10.1016/j.sedgeo.2006.05.013.

313 Smith, A. G., Hurley, A. M., and Briden, J. C. (1981). Phanerozoic paleocontinental world maps (Vol.
314 102). Cambridge: Cambridge University Press, 102 p.

315 Sprain, C. J., Renne, P. R., Vanderkluysen, L., Pande, K., Self, S., and Mittal, T., 2019, The eruptive tempo
316 of Deccan volcanism in relation to the Cretaceous-Paleogene boundary: Science, v. 363, p. 866-
317 870, doi: 10.1126/science.aav1446.

318 Sutton, R. T., Dong, B., and Gregory, J. M., 2007, Land/sea warming ratio in response to climate change:
319 IPCC AR4 model results and comparison with observations: Geophysical Research Letters, v. 34,
320 L02701, doi: 10.1029/2006gl028164.

Sweet, A. R., and Braman, D. R., 1992, The KT boundary and contiguous strata in western Canada: interactions between paleoenvironments and palynological assemblages: Cretaceous Research, v. 13, p. 31-79, doi: 10.1016/0195-6671(92)90027-N.

Tabor, C. R., Poulsen, C. J., Lunt, D. J., Rosenbloom, N. A., Otto-Bliesner, B. L., Markwick, P. J., Brady, E.C., Farnsworth, A., and Feng, R., 2016, The cause of Late Cretaceous cooling: A multimodel-proxy comparison: Geology, v. 44, p. 963-966, doi: 10.1130/G38363.1.

Taylor, K. W., Willumsen, P. S., Hollis, C. J., and Pancost, R. D., 2018, South Pacific evidence for the long-term climate impact of the Cretaceous/Paleogene boundary event: Earth-Science Reviews, v. 179, p. 287-302, doi: 10.1016/j.earscirev.2018.02.012.

van Hinsbergen, D. J., De Groot, L. V., van Schaik, S. J., Spakman, W., Bijl, P. K., Sluijs, A., Langereis, C.G., and Brinkhuis, H., 2015, A paleolatitude calculator for paleoclimate studies: PloS one, v. 10, e0126946, doi: 10.1371/journal.pone.0126946.

Vellekoop, J., Esmeray-Senlet, S., Miller, K. G., Browning, J. V., Sluijs, A., van de Schootbrugge, B., Damsté, J.S.S., and Brinkhuis, H., 2016, Evidence for Cretaceous-Paleogene boundary bolide "impact winter" conditions from New Jersey, USA: Geology, v. 44, p. 619-622, doi: 10.1130/G37961.1.

Vellekoop, J., Sluijs, A., Smit, J., Schouten, S., Weijers, J. W., Sinninghe Damsté, J. S., and Brinkhuis, H., 2014, Rapid short-term cooling following the Chicxulub impact at the Cretaceous–Paleogene boundary: Proceedings of the National Academy of Sciences, v. 111, p. 7537-7541, doi: 10.1073/pnas.1319253111.

Vickers, M. L., et al., 2020, Cold spells in the Nordic Seas during the early Eocene Greenhouse: Nature Communications, v. 11, p. 1-12, doi:0.1038/s41467-020-18558-7.

Weijers, J. W., Schouten, S., van den Donker, J. C., Hopmans, E. C., and Damsté, J. S. S., 2007, Environmental controls on bacterial tetraether membrane lipid distribution in soils: Geochimica et Cosmochimica Acta, v. 71, p. 703-713, doi: 10.1016/j.gca.2006.10.003.

Zhang, L., Hay, W. W., Wang, C., and Gu, X., 2019, The evolution of latitudinal temperature gradients from the latest Cretaceous through the Present: Earth-Science Reviews, v. 189, p. 147-158, doi: 10.1016/j.earscirev.2019.01.025.

SUPPLEMENTARY MATERIAL

Site description and sampling

The Ferris Coal at Wood Mountain Creek (49°25'20"N 106°19'50"W) and Rock Creek West (49°02'20"N 106°34'00") has been shown to span the K-Pg boundary, based on the distinctive 1–2 cm thick pink- to buff-coloured Ir-enriched claystone contained in each section (Nichols et al. 1986; Sweet and Braman 1992). The claystone is also coincident with a palynologically defined extinction of Cretaceous flora (Sweet and Braman 1992). At the time of the K-Pg boundary, the sites were (1) peat mires accumulating in the foreland basin of the ancestral Rocky Mountains (Jerrett et al. 2015); (2) inland, approximately equidistant between the shorelines of the (proto) Gulf of Mexico and the Boreal Sea (now the Arctic Ocean; Fig. 1); (3) at a palaeolatitude of approximately 54–56°N (van Hinsbergen et al. 2015); and (4) at negligible altitude, as evidenced by the persistence of marine conditions in the Maastrichtian Bearpaw Formation some tens of metres below the K-Pg boundary (Sweet and Braman, 2001). Vitrinite reflectance data (R_o) values for the Ferris Coal at the sites are <0.38%, indicating lignite rank (Bustin 1991), and ensuring the preservation of GDGTs (Schouten et al. 2004; 2013).

At both sites, the entire coal seam was contiguously sampled. Wood Mountain Creek was sampled in 2011 (56 samples). Sampling methodology and $\delta^{13}C_{org}$ analyses were previously published in Jerrett et al. (2015) and the latter are re-reported in Supplementary Table S1. Remaining material

from the Wood Mountain Creek site were used for brGDGT analysis in this study. Rock Creek West was sampled in 2019 (36 samples), using the same methods as described in Jerrett et al. (2015).

Geochemical analysis and brGDGT method validation

All samples were freeze-dried and finely ground using a granite pestle and mortar prior to geochemical analyses.

Wood Mountain Creek

Approximately 0.5 g of sediment was solvent-extracted using ~20mL of DCM/methanol (9:1, v/v) in a Milestone Ethos Ex microwave extraction system at the Organic Geochemistry Unit (OGU) at the University of Bristol. Temperature in the microwave was programmed to increase linearly from room temperature to 70°C over 10 min at which it was held for 10 min, and then cooled to room temperature over 20 minutes. The total lipid extract (TLE) was dissolved in hexane:propanol (99:1, v/v) and filtered (0.45 µm PTFE) prior to analysis.

Samples were analysed for their GDGT content by high-performance liquid chromatography/atmospheric pressure chemical ionization–mass spectrometry (HPLC/APCI-MS) at the University of Bristol using a ThermoFisher Scientific Accela Quantum Access. Normal-phase separation was achieved following the method of Naafs et al. (2017a), which includes using two UHPLC silica columns for compound separation. Selective ion monitoring (SIM) was used to detect the $[M+H]^+$ ions of the following masses: *m/z* 1292, 1050, 1048, 1046, 1036, 1034, 1032, 1022, 1020, 1018, 744). The average standard deviation for duplicate MBT' measurements of an in-house standard was 0.026 units. The data are reported in Supplementary Table S1. The MBT'5Me index was calculated following De Jonge et al. (2014):

$$\mathrm{MBT'5Me} = \frac{[\mathrm{Ia}] + [\mathrm{Ib}] + [\mathrm{Ic}]}{[\mathrm{Ia}] + [\mathrm{Ib}] + [\mathrm{Ic}] + [\mathrm{IIa}] + [\mathrm{IIb}] + [\mathrm{IIc}] + [\mathrm{IIIa}]}$$

The peat specific calibration ($MAAT_{peat}$, Naafs et al. 2017a) was used to convert MBT'5Me values into mean annual air temperatures:

$$\mathrm{MAAT_{peat}}\ (°\mathrm{C}) = 52.18(\mathrm{MBT'5Me}) - 23.05$$

The CBT_{peat} index was calculated following De Jonge et al. (2014):

$$CBT_{peat} = \log\frac{Ib + IIa' + IIb + IIb' + IIIa'}{Ia + IIa + IIIa}$$

The CBT_{peat} values were converted into pH following Naafs et al. (2017a):

$$\mathrm{pH} = 2.29\left(\mathrm{CBT_{peat}}\right) + 8.07$$

Rock Creek West

For $\delta^{13}C_{org}$ analysis, samples were oven dried (30°C, 24 h), and decarbonated using hydrochloric acid (10% v/v) until any visible reaction had ceased. The samples were then repeatedly washed with deionised water until a neutral solution was obtained, and oven dried again (30°C, 24 h). Carbon isotope analyses were conducted at the University of Plymouth using a Thermo Scientific Delta V Advantage. Carbon-isotope ratios are expressed using the internationally accepted per mil (‰) standard notation relative to the Vienna Peedee belemnite (VPDB) standard (Table S1). Instrument calibration was achieved using three international standards: USGS 40 (l-glutamic acid, $\delta^{13}C$ = -26.389‰), USGS 24 (graphite, $\delta^{13}C$ = -16.049‰), and IAEA CH-7 (polyethylene, $\delta^{13}C$ = -32.151‰). The standard deviation on replicates in run analyses of the USGS 40 standard was ±0.12‰.

Approximately 1 g of sediment was solvent-extracted using 20mL of DCM/methanol (9:1, v/v) in a microwave assisted reactor system (MARS 6, CEM) at the University of Manchester following the same protocol as for Wood Mountain Creek. The TLE was separated into polar and apolar fractions by column chromatography, using hexane/DCM (9:1, v/v) and DCM/methanol (1:1, v/v) respectively as the eluents, and Al_2O_3 as the stationary phase. The polar fraction was re-dissolved in hexane/propanol (99:1, v/v) and filtered using a 0.45 µm PTFE filter prior to analysis.

Analysis of GDGTs was carried out using a Dionex LPG-U3400(SDN) UHPLC liquid chromatography system and Thermo Scientific Q Exactive Focus mass spectrometer with Atmospheric Pressure Chemical Ionisation (APCI) at the University of Plymouth. For the determination of MBT'5Me, the method of Hopmans et al. (2016) was adapted to this high-performance instrument employing a single Waters Acquity UPLC, BEH HILIC 1.7 µm (150 x 2.1 mm, 1.7 µm) column and precolumn at 40°C. Using solvents A (hexane) and B (9:1 hexane:isopropanol v/v) and a flow of 600 µl min -1, the mix started at 5% B (isocratic from 0–3 min), rising to 18 % B at 5 min (isocratic 5–10 min), rising to 35% B at 15 min and 100% B at 17.4 min, with 2.6 min re-equilibration time, which slightly shortened the analysis time. APCI was carried out in positive polarisation mode, at a capillary temperature of 275°C. Masses were scanned from *m/z* 200 to 2000, and resolved to 70,000 at *m/z* 200, with mass calibration carried out externally in electro spray ionisation mode, using auto-calibration Pierce LTQ Velos ESI positive ion calibration solution (n-butylamine, caffeine, MRFA, and Ultramark 1621). GDGTs were identified based on retention times and accurate masses: using 1022.00967 (brGDGT-Ia), 1019.99402 (brGDGT-Ib), 1017.97837 (brGDGT-Ic), 1036.02532 (brGDGT-IIa+IIa'), 1034.00967 (brGDGT-IIb+IIb'), 1031.99402 (brGDGT-IIc+IIc'), 1050.04097 (brGDGT-IIIa+IIIa'), 1048.02532 (brGDGT-IIIb+IIIb'), 1046.00967 (brGDGT-IIIc+IIIc'), and 1292.24442 (crenarchaeol). Integration was carried out using Xcalibur 4.2 using QuanBrowser integration and data management. The data are reported in Supplementary Table S1. Temperature and pH were calculated using the same equations as for Wood Mountain Creek.

Comparison of HPLC data from University of Bristol and Plymouth University

To allow comparability between the samples analysed at the University of Bristol and the University of Plymouth, in particular for 6-Me separation, a set of standards and unrelated, representative samples, were analyzed at Bristol and Plymouth (marine standard and EH-8, Lengger et al. 2018). Further, as the HPLC-APCI-MS method for GDGT analyses was shortened to allow higher

sample-throughput, taking advantage of the UHPLC-Orbitrap-MS system at the University of Plymouth, a subset of standards and samples were run on both methods ('long' for standard method acc. to Hopmans et al. (2016), 'short' method for 20 min method: shown are marine standard and EH-8 as described in Lengger et al. (2018); RCW-26 this work), to determine reproducibility (Fig. S1). The 'short' method is a variation of Hopmans et al. (2016), modified to run on one HPLC column (not two), and completes a sample run in 20 minutes (described in Vickers et al. 2020). As a result, the resolution is slightly compromised when compared to Hopmans et al. (2016), though the resolution of the 'short' method is comparable to the method at the University of Bristol (Fig. S1). The results from both 'short' and 'long' methods are very similar, with similar MBT' and MBT'5Me values calculated for both (Table S2). In addition, the 'long' method was also implemented at Plymouth and used for cross-calibration.

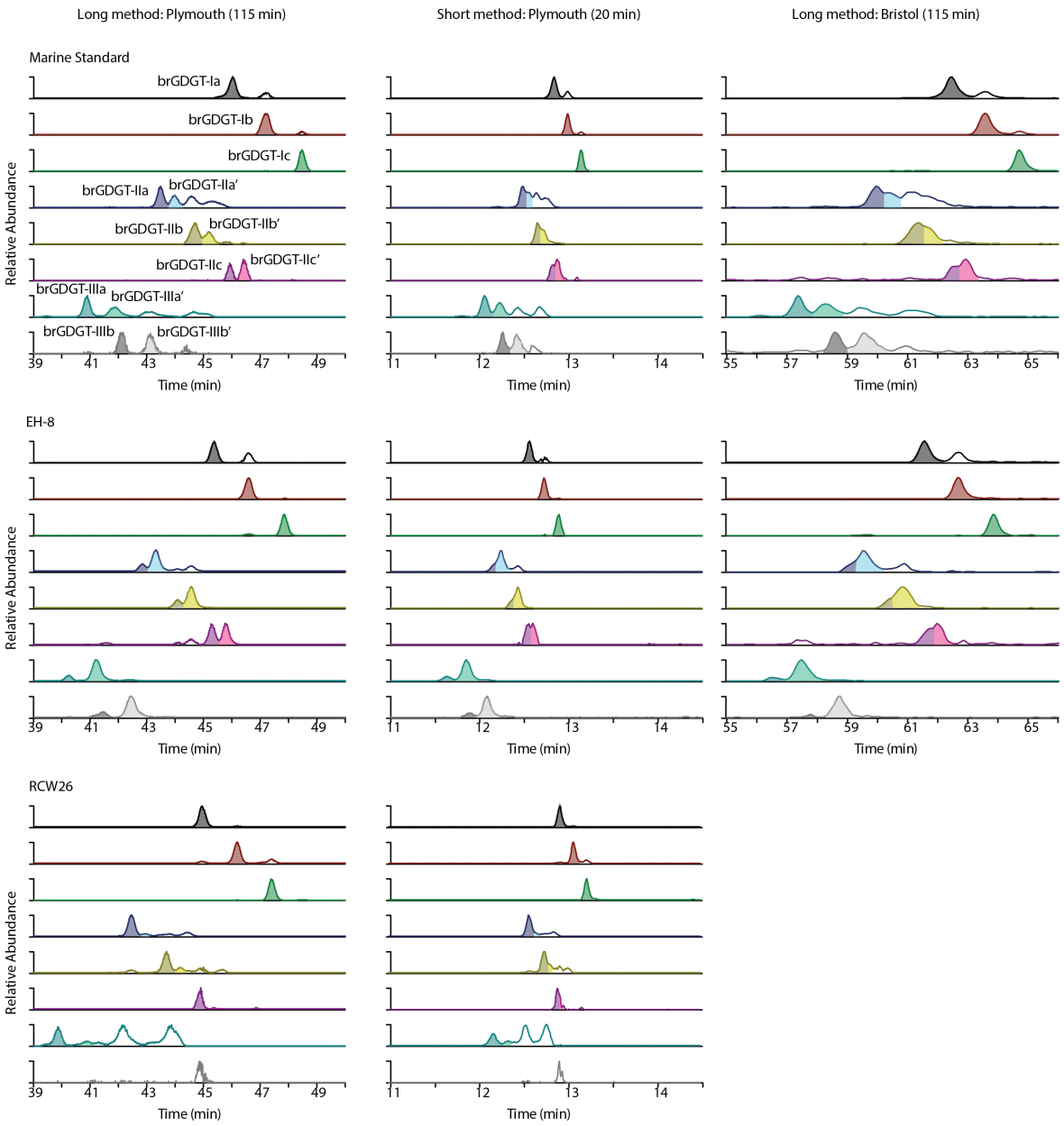

Supplementary figure S1. *Chromatograms showing the difference in resolution of individual brGDGTs and their isomers in the 'Long' method at Plymouth University (A), the 'Short' method at Plymouth University (B), and the 'Long' method at University of Bristol. 6-methyl-GDGTs are indicated with '.*

Fidelity of the MAAT record

Where possible, all GDGT analyses were duplicated (Table S1). A minority either could not be analysed a second time or showed a standard deviation >1 due to the low concentration of brGDGTs, and these samples and

were eliminated from the study (Table S1). Shale samples were also excluded as the peat-specific calibration is not tested in shales. We note that the proxy is at or close to saturation (MBT'_{5me} = 1) in a small number of retained datapoints.

To explore the fidelity of our GDGT-reconstructed temperatures, we examined the distributions of other GDGTs and biomarkers indicative of depositional environment. Previous work has shown that major changes in depositional setting, as inferred from reconstructed pH, can bias temperature estimates (Weijers et al. 2011; Inglis et al. 2019). Chen et al. (2022) and Halamka et al. (2022) showed that in the Acidobacterium Solibacter usitatus, the only organism known to produce a suite of brGDGTs comparable to that seen in the environment, the degree of methylation (captured in the MBT'5Me index) is correlated to MAAT but the degree of cyclisation (captured in the CBT' and CBTpeat indices) is not correlated to pH. This finding prompted the former to suggest that the degree of cyclisation-pH relationship is based on changes in community structure rather a physiological response; if so, that change in community structure could also affect the MBT'5Me-MAAT relationship, accounting for previous observations (De Jonge et al. 2021). Subsequent work (Rao et al., 2022) further suggests that changes in water depth in wetlands could also affect the MBT'5Me-MAAT relationship.

In the studied sections, CBT_{peat}-pH does vary (from 4.4 to 6.8; Table S1), though at neither Rock Creek West nor Wood Mountain Creek do these variations correlate with temperature changes. At Rock Creek West there is a decline in pH from 7 to 6.5 from the basal (Cretaceous) parts to the lowermost (Paleogene) parts of the coals, and thereafter pH varies between 5 and 6. At Wood Mountain Creek, the pH is highly variable in the Cretaceous (from 4.4 to 6.3), but in the earliest Paleogene declines from 6.5, and thereafter varies between 5 and 6. The patterns are consistent with palynological (Sweet and Braman 1992) and petrographic (Sweet and Cameron 1991; Jerrett et al. 2015) data that imply that the coal at both sites represents a hydroseral succession upwards from (typically more alkaline) ponded, disconnected forested rheotrophic mires in-filling topographic hollows, to (typically more acidic) aerially expansive herbaceous, possibly ombrotrophic mires. We observe no correlation between pH and temperature, and there is no change in CBT associated with

485 the post-boundary cooling. Although the variations in CBT-derived pH are larger than those observed
486 in other lignite settings (e.g., Lauretano et al. 2021), they are smaller than the previous studies where
487 pH was inferred to bias temperature estimates (Weijers et al. 2011; Inglis et al. 2019). Moreover, at
488 Rock Creek West, the clear decline in post-boundary temperatures is associated with near-constant
489 pH values. Some of the smaller variations in pH do coincide with changes in reconstructed
490 temperature, however, and we therefore focus on the main trends in MAAT.

491 Further evidence for relatively stable environmental conditions comes from the BIT index
492 (Hopmans et al. 2004), which reflects the relative abundance of brGDGTs to crenarchaeol, an isoGDGT
493 produced by soil and aquatic Thaumarchaeota. BIT values are typically >0.99, again consistent with a
494 persistent peatland setting, but in a few intervals values decline to 0.97 (Table S1). Zheng et al (2015)
495 showed that intervals of severe peatland drying are associated with increases in the fractional
496 abundance of crenarchaeol relative to isoGDGTs. Wood Mountain Creek appears to have experienced
497 such episodes just above and below the KPg Boundary (Table S1); however, these do not coincide with
498 temperature change. The isoGDGT:brGDGT ratio at Wood Mountain Creek is somewhat variable
499 throughout and shows no relationship with temperature. Rock Creek West shows increased
500 crenarchaeol abundance near the top of the section, coincident with an interval of greater
501 isoGDGT:brGDGT ratios and the coolest temperatures recorded at this site. These changes suggest a
502 relationship between cooling and apparent peatland drying but this speculation requires further
503 investigation.

504 To further explore the wider biomarker distribution at these sites, we determined the bacterial
505 hopane isomerisation ratio. Isomerisation at the C_{17} and C_{21} positions (from the 17□,21□(H) to the
506 17□,21□(H) configuration) normally occurs with increasing thermal maturity over millions of years
507 (Mackenzie et al. 1980), but this process is accelerated, especially for the C_{31} hopane, under acidic
508 conditions in wetlands. Recent work showed that the degree of isomerisation for the C_{31} hopane in
509 wetlands provides an independent method to reconstruct pH (Inglis et al. 2018, 2019).

The apolar fractions were analysed using an Agilent 7890A gas chromatograph (GC) interfaced to an Agilent 5975C MSD mass spectrometer (MS) operated in electron ionisation scan/SIM mode (scanning range, *m/z* 50–600; SIM masses used: *m/z* 57, 66, 191 and 205; ionisation energy, 70 eV; solvent delay of 2.5 min) using helium as the carrier gas at a constant flow (1 mL/min). The GC was equipped with an Agilent 7683B auto-sampler and programmable temperature vaporization (PTV) inlet. The samples were dissolved in hexane prior to injection, injected using pulsed split-less injection (1 µL; inlet pressure of 25 psi for 0.75 min), and separated on a Zebron ZB-5MS capillary column (Phenomenex; length 30 m; 250 µm ID, 0.25 µm film thickness). The heated interface (MSD transfer line) and PTV temperatures were set to 280°C, the mass source, at 230°C and the mass spectrometer quadrupole at 150°C. The samples were injected at 50°C and the oven was programmed to ramp to 130°C at 20°C/min and then to 310°C at 6°C/min, at which it was kept isothermally for 15 min. Compounds were identified by comparison of their mass fragments (*m/z*) with The National Institute of Standards and Technology (NIST) library. Quantitative data were determined by comparison of individual peak areas with a known concentration of the internal standard deuterated tetracosane, added prior to analyse and pH was calculated using the C_{31} hopanes following Inglis et al. (2018):

$$\mathrm{pH} = 5.22 \left(C_{31}\ hopane\ \frac{\beta\beta}{\alpha\beta\ +\ \beta\beta} \right) + 3.11$$

Overall values of the C_{31} ββ /(αβ + ββ) hopane ratio range between 0.06 and 0.42, translating in to pH values between 3.4 and 5.3. These values are lower compared to the brGDGT-based estimates, but consistent with an acidic peat forming environment.

Another unusual feature of the brGDGT distribution of these sections is the lack of 6'-methyl brGDGTs in nearly all samples despite reconstructed pH between 7 and 4. At such pH and especially above pH 6, 6'-methyl brGDGTs do occur in modern mineral soils and peatlands (Naafs et al. 2017a, 2017b). This is not an artefact of the analytical method, as we cross-checked with the “long” method in Plymouth (Fig. S1). Therefore, we interpret our MAAT record cautiously, focusing primarily on the most pronounced variations which are not correlated with changes in CBT. That is, peak temperatures

535 immediately above the K-Pg boundary, and the long-term decline in MAATs in the Paleogene part of
536 the record.

537

538 **Age Model**

539 *Correlation:* First order correlation between the two sites is based on the occurrence of the
540 distinctive Ir-bearing claystone that is also palynologically enriched in fern spores (Sweet and Braman,
541 1992), and marks the base of the Paleogene. Its base is used as a horizontal datum in Figure 2 and
542 Figure S2. Jerrett et al. (2015) interpreted these coals to represent, at least in part, small, disconnected
543 rheotrophic mires, readily subject to local autogenic clastic input. Consequently, a lithostratigraphic
544 approach would not be appropriate for the generation of other chronostratigraphic tie-points in this
545 case. Instead, secondary tiepoints are provided by inflexion points on their respective $\delta^{13}C_{org}$
546 stratigraphies of the two sites (Tiepoints 1–9; Figs. 2 and S2). These can be interpreted as representing
547 a more regional stratigraphic signal relating to changes in the carbon isotopic composition of the
548 atmosphere the plants in the peats were metabolising (Arens and Jahren, 2000). This correlation is
549 consistent with an independent correlation between the two sites based on petrographic criteria by
550 Jerrett et al. (2015).

551 *Timescales:* Estimations of the duration of time represented by such short stratigraphies are
552 difficult. Broad estimates of the duration of time represented by the two coal seams, however, can be
553 estimated from the absolute age determinations of Renne et al. (2013) at the coal-bearing K-Pg site at
554 Hell Creek Marina Road (Montana), located 170 km SSW of Rock Creek West (Fig. 1). The stratigraphy
555 of the site is represented by 160 cm of coal, which directly overlies the Ir-enriched claystone marking
556 the K-Pg boundary. The coal contains two tuffs termed Z2 and Z1, 80 cm and 120 cm above the K-Pg
557 boundary, respectively. $^{40}Ar/^{39}Ar$ dating of sanidines in the tuffs yield an age of 66.019 ±0.021 Ma for
558 Z2, and 66.003 ±0.033 Ma for Z1 (Renne et al. 2013), giving a most likely duration of 16 ka for the
559 40 cm of intervening coal (i.e., 1 m represents 40 ka). Error estimates of the ages suggest a maximum

possible duration of 90 ka is possible for the 40 cm of intervening coal (i.e., 1 m represents 175 ka), and an unlikely minimum duration that equates to instantaneous deposition. Compilations of Holocene peat accumulation rates show that long-term, time averaged peat accumulation rates decrease by half an order of magnitude from Tropics to high latitudes (Diessel et al. 2000). We consider the distance between Hell Creek Road, whence we derive our peat accumulation rates, and our Saskatchewan sites to represent negligible latitudinal difference. It therefore provides the best, and a realistic age model for our sites, in the absence of such radiometric data at the study locations.

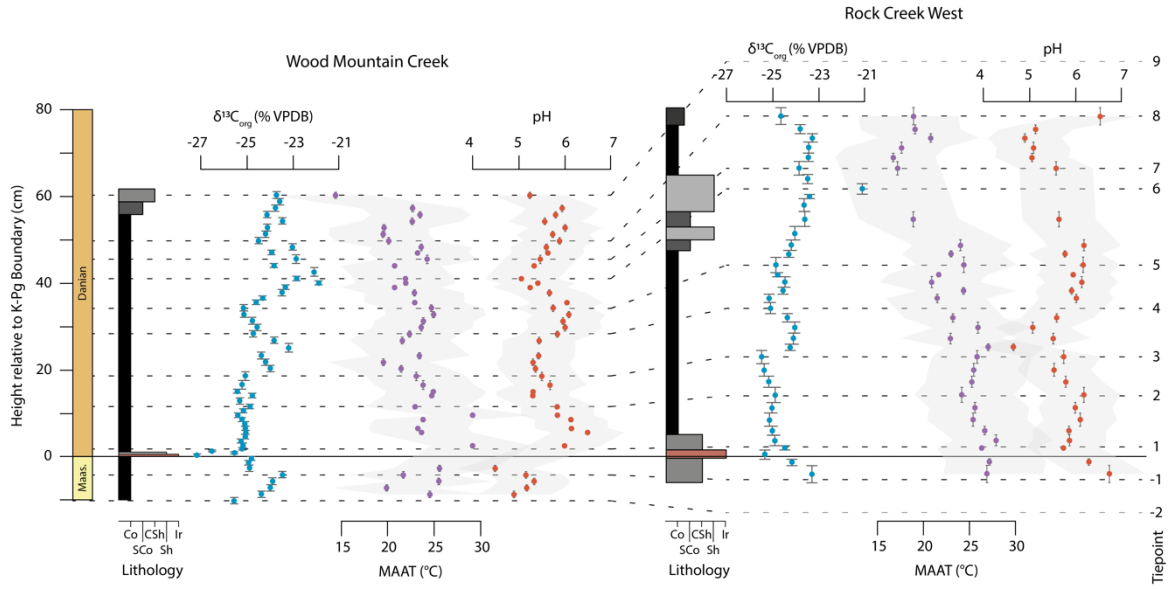

Supplementary figure S2. *$\delta^{13}C_{org}$ (blue), brGDGT mean annual air temperature (MAAT; purple), CBT_{peat}-pH (red) records from Wood Mountain Creek and Rock Creek West, Saskatchewan, plotted against height relative to the K-Pg boundary. Vertical error bars show the stratigraphic range of each sample. Dashed lines show chemostratigraphic ($\delta^{13}C_{org}$) correlation tiepoints. Solid line shows the Ir-claystone K-Pg datum. On the lithology log, Co = coal, ShC = shaley coal, CSh = coaly shale, Sh = shale, and Ir = iridium-enriched claystone.*

In Supplementary Table S3, the most likely (1 m = 40 ka), minimum (1 m = 0 ka), and maximum (1 m = 175 ka) duration of time represented by the coal is used to date Tiepoints 1–9, relative to the K-Pg boundary (Fig. 2 and S3). Differences in thicknesses of coal between the tiepoints (i.e., differences in thicknesses of the $\delta^{13}C_{org}$ excursion stratigraphies) at Rock Creek West and Wood Mountain Creek (Fig. 2 and S2) clearly imply that there were differences in synchronous peat accumulation rates and/or post-depositional compaction of the peat at the two sites (and also between these sites and the Hell Creek Marina Road site of Renne et al. 2013). These differences highlight uncertainties, but the approach places clear absolute errors in the timescales of MAAT change interpreted in this study. The ages relative to the K-Pg boundary that we use for Tiepoints 1–9 are based on the average determined for Rock Creek West, and Wood Mountain Creek (Table S3).

Having established the best-estimate ages of Tiepoints 1–9 (Table S3), the midpoint of each sample was linearly extrapolated between the ages of the Tiepoints to ascribe each an individual age relative to the K-Pg boundary (Table S4). MAAT for each datapoint were plotted against these ages to make Figure 3.

TABLE CAPTIONS

Supplementary Table S1. *Stratigraphic and lithological data, GDGT abundances, proxy calculations (MBT'5Me, MAAT, CBT_{peat}, pH, and hopane ratio), and $\delta^{13}C_{org}$ for all samples reported in this study. MBT'5Me (Columns AH, BJ, BQ) calculated from De Jonge et al. (2015). MAAT (Columns AI, BK, BR) calculated from Naafs et al. (2017a). CBT_{peat} (Columns AJ, BL, BT) calculated from Naafs et al. (2018). pH (Columns AK, BM, BU) calculated from Naafs et al. (2018). Hopane ratio (Column BV) calculated from Inglis et al. (2018). Blank cells (columns J–AC, AL–BE) denote below the detection limit/unquantifiable GDGTs. The $\delta^{13}C_{org}$ values (columns BX–CE) for Wood Mountain Creek are from Jerrett et al. (2015). All other data was generated for this study. Where the standard deviation of MAAT > 1, this sample was omitted from the study. Where polar fraction analysis not undertaken or duplicated, this sample was omitted from the study.*

Supplementary Table S2*. Comparison of MBT, MBT'5Me proxy values calculated from the 'Short' and 'Long' HPLC-APCI-MS methods at Plymouth University and the 'long' method at the University of Bristol. (std= standard, RCW= Rock Creek West, SD= standard deviation).*

Supplementary Table S3. *Age of Tiepoints 1–9 (Fig. S2) at Rock Creek West and Wood Mountain Creek relative to the K-Pg boundary (columns C–E and G–I respectively), applying the minimum (1 m = 0 ka), most likely (1 m = 40 ka), and maximum (1 m = 175 ka) duration of time represented by the coal from Renne et al. (2013). Also shown are the average relative ages of the tiepoints from Rock Creek West and Wood Mountain Creek (columns L-N). The most likely duration of the average tiepoint ages (column M) are the values used to generate the ages for each datapoint in Supplementary Table S4.*

Supplementary Table S4. *All samples, and their assigned ages generated through linear interpolation of the position of their midpoint between tiepoints. The ages of the tiepoints are from column M (Supplementary Table S3). Also shown are the MAAT (°C) and mean* $\delta^{13}C$ *(‰) values from Supplementary Table S1. These data are used to plot Figure 3.*

Supplementary Table S5. *Statistical analysis of MAAT data. MAAT data were separated into four temporal bins: pre-K-Pg boundary (-5–0 ka), 0–10 ka, 10–20 ka, and 20–30 ka. These bins were then analysed using two-sample, equal variances t-tests to determine the statistical significance of temperature trends. These data are included in Figure 3.*

Supplementary references

Arens, N.C., Jahren, A.H., and Amundson, R., 2000, Can C3 plants faithfully record the isotopic composition of atmospheric carbon dioxide?: Paleobiology, v. 26, p. 137–164, doi: 10.1666/0094-8373(2000)026<0137:CCPFRT>2.0.CO;2.

Bustin, R. M., 1991, Organic maturity in the western Canada sedimentary basin: International Journal of Coal Geology, v. 19, p. 319-358, doi: 10.1016/0166-5162(91)90026-F.

De Jonge, C., Kuramae, E. E., Radujković, D., Weedon, J. T., Janssens, I. A., and Peterse, F., 2021, The influence of soil chemistry on branched tetraether lipids in mid-and high latitude soils:

628 Implications for brGDGT-based paleothermometry: Geochimica et Cosmochimica Acta, v. 310,
629 p. 95-112, doi: 10.1016/j.gca.2021.06.037.

630 Diessel, C., Boyd, R., Wadsworth, J., Leckie, D., and Chalmers, G., 2000, On balanced and unbalanced
631 accommodation/peat accumulation ratios in the Cretaceous coals from Gates Formation,
632 Western Canada, and their sequence-stratigraphic significance: International Journal of Coal
633 Geology, v. 43, p. 143-186, doi: 10.1016/S0166-5162(99)00058-0.

634 Hopmans, E. C., Weijers, J. W., Schefuß, E., Herfort, L., Damsté, J. S. S., and Schouten, S., 2004, A novel
635 proxy for terrestrial organic matter in sediments based on branched and isoprenoid tetraether
636 lipids: Earth and Planetary Science Letters, v. 224, p. 107-116, doi: 10.1016/j.epsl.2004.05.012.

637 Hopmans, E. C., Schouten, S., and Damsté, J. S. S., 2016, The effect of improved chromatography on
638 GDGT-based palaeoproxies: Organic Geochemistry, v. 93, p. 1-6, doi:
639 10.1016/j.orggeochem.2015.12.006.

640 Inglis, G. N., Farnsworth, A., Collinson, M. E., Carmichael, M. J., Naafs, B. D. A., Lunt, D. J., Valdes, P.J.
641 and Pancost, R.D., 2019, Terrestrial environmental change across the onset of the PETM and
642 the associated impact on biomarker proxies: A cautionary tale: Global and Planetary Change, v.
643 181, 102991, doi: 10.1016/j.gloplacha.2019.102991.

644 Inglis, G. N., Naafs, B. D. A., Zheng, Y., McClymont, E. L., Evershed, R. P., and Pancost, R. D., 2018,
645 Distributions of geohopanoids in peat: Implications for the use of hopanoid-based proxies in
646 natural archives: Geochimica et Cosmochimica Acta, v. 224, p. 249-261, doi:
647 10.1016/j.gca.2017.12.029.

648 Jerrett, R. M., Price, G. D., Grimes, S. T., Dawson, A. T., 2015, A paleoclimatic and paleoatmospheric
649 record from peatlands accumulating during the Cretaceous-Paleogene boundary event,
650 Western Interior Basin, Canada: Geological Society of America Bulletin, v. 127, p. 1564–1582;
651 doi: 10.1130/B31166.1.

652 Lauretano, V., Kennedy-Asser, A. T., Korasidis, V. A., Wallace, M. W., Valdes, P. J., Lunt, D. J., Pancost,
653 R.D., and Naafs, B. D. A., 2021, Eocene to Oligocene terrestrial Southern Hemisphere cooling
654 caused by declining pCO2: Nature Geoscience, v. 14, p. 659-664, doi: 10.1038/s41561-021-
655 00788-z.

656 Lengger, S. K., Sutton, P. A., Rowland, S. J., Hurley, S. J., Pearson, A., Naafs, B. D. A., Dang, X., Inglis,
657 G.N., and Pancost, R. D., 2018, Archaeal and bacterial glycerol dialkyl glycerol tetraether (GDGT)
658 lipids in environmental samples by high temperature-gas chromatography with flame ionisation
659 and time-of-flight mass spectrometry detection: Organic Geochemistry, v. 121, p. 10-21, doi:
660 10.1016/j.orggeochem.2018.03.012.

661 Mackenzie, A.S., Patience, R.L., Maxwell, J.R., Vandenbroucke, M., Durand, B., 1980, Molecular
662 parameters of maturation in the Toarcian shales, Paris Basin, France—I. Changes in the
663 configurations of acyclic isoprenoid alkanes, steranes and triterpanes: Geochimica et
664 Cosmochimica Acta, v. 44, p. 1709-1721, doi: 10.1016/0016-7037(80)90222-7.

665 Naafs, B.D.A., Inglis, G.N., Zheng, Y., Amesbury, M.J., Biester, H., Bindler, R., Blewett, J., Burrows, M.A.,
666 Del Castillo Torres, D., Chambers, F.M., et al., 2017a, Introducing global peat-specific
667 temperature and pH calibrations based on brGDGT bacterial lipids: Geochimica et
668 Cosmochimica Acta, v. 208, p. 285-301, doi: 10.1016/j.gca.2017.01.038.

669 Naafs, B.D.A., Gallego-Sala, A.V., Inglis, G.N., Pancost, R.D., 2017b. Refining the global branched
670 glycerol dialkyl glycerol tetraether (brGDGT) soil temperature calibration. Organic
671 Geochemistry, v. 106, p. 48-56, doi: 10.1016/j.orggeochem.2017.01.009.

672 Naafs, B. D. A., Rohrssen, M., Inglis, G. N., Lähteenoja, O., Feakins, S. J., Collinson, M. E., Kennedy, E.M.,
673 Singh, P.K., Singh, M.P., Lunt, D.J., et al., 2018, High temperatures in the terrestrial mid-latitudes
674 during the early Palaeogene: Nature Geoscience, v. 11, p. 766-771, doi: 10.1038/s41561-018-
675 0199-0.

Nichols, D. J., Jarzen, D. M., Orth, C. J., and Oliver, P. Q., 1986, Palynological and iridium anomalies at Cretaceous-Tertiary boundary, south-central Saskatchewan: Science, v. 231, p. 714-717, doi: 10.1126/science.231.4739.71.

Rao, Z., Guo, H., Wei, S., Cao, J., and Jia, G., 2022, Influence of water conditions on peat brGDGTs: A modern investigation and its paleoclimatic implications: Chemical Geology, v. 606, 120993, doi: 10.1016/j.chemgeo.2022.120993.

Renne, P. R., Deino, A. L., Hilgen, F. J., Kuiper, K. F., Mark, D. F., Mitchell III, W. S., Morgan, L.E., Mundil, R. and Smit, J., 2013, Time scales of critical events around the Cretaceous-Paleogene boundary: Science, v. 339, p. 684-687, doi: 10.1126/science.1230492.

Schouten, S., Hopmans, E.C., Sinninghe Damsté, J.S., 2004, The effect of maturity and depositional redox conditions on archaeal tetraether lipid palaeothermometry: Organic Geochemistry v. 35, p. 567-571, doi: 10.1016/j.orggeochem.2004.01.012.

Schouten, S., Hopmans, E.C., Sinninghe Damsté, J.S., 2013, The organic geochemistry of glycerol dialkyl glycerol tetraether lipids: A review: Organic Geochemistry, v. 54, p. 19-61, doi: 10.1016/j.orggeochem.2012.09.006.

Sweet, A. R., and Braman, D. R., 2001, Cretaceous–Tertiary palynofloral perturbations and extinctions within the *Aquilapollenites* Phytogeographic Province: Canadian Journal of Earth Sciences, v. 38, p. 249-269, doi: 10.1139/e00-024.

Sweet, A. R., and Cameron, A. R., 1991, Palynofacies, coal petrographic facies and depositional environments: Amphitheatre Formation (Eocene to Oligocene) and Ravenscrag Formation (Maastrichtian to Paleocene), Canada: International Journal of Coal Geology, v. 19, p. 121-144, doi: 10.1016/0166-5162(91)90017-D.

698 Sweet, A. R., and Braman, D. R., 1992, The KT boundary and contiguous strata in western Canada:
699 interactions between paleoenvironments and palynological assemblages: Cretaceous Research,
700 v. 13, p. 31-79, doi: 10.1016/0195-6671(92)90027-N.

701 van Hinsbergen, D. J., De Groot, L. V., van Schaik, S. J., Spakman, W., Bijl, P. K., Sluijs, A., Langereis,
702 C.G., and Brinkhuis, H., 2015, A paleolatitude calculator for paleoclimate studies: PloS one, v.
703 10, e0126946, doi: 10.1371/journal.pone.0126946.

704 Vickers, M. L., Lengger, S. K., Bernasconi, S. M., Thibault, N., Schultz, B. P., Fernandez, A., Ullmann,
705 C.V., McCormack, P., Bjerrum, C.J., Rasmussen, J.A., et al., 2020, Cold spells in the Nordic Seas
706 during the early Eocene Greenhouse: Nature Communications, v. 11, p. 1-12, doi:
707 0.1038/s41467-020-18558-7.

708 Weijers, J. W., Schouten, S., van den Donker, J. C., Hopmans, E. C., and Damsté, J. S. S., 2007,
709 Environmental controls on bacterial tetraether membrane lipid distribution in soils: Geochimica
710 et Cosmochimica Acta, v. 71, p. 703-713, doi: 10.1016/j.gca.2006.10.003.

711 Zheng, Y., Li, Q., Wang, Z., Naafs, B. D. A., Yu, X., and Pancost, R. D., 2015, Peatland GDGT records of
712 Holocene climatic and biogeochemical responses to the Asian Monsoon: Organic Geochemistry,
713 v. 87, p. 86-95, doi: 10.1016/j.orggeochem.2015.07.012.